

Experimental and Computational Investigation of the Influence of Ethanol on Auto-ignition of *n*-Heptane in Non-Premixed Flows

Liang Ji, Kalyanasundaram Seshadri*, Forman A. Williams

University of California at San Diego, La Jolla, California 92093-0411, USA

Abstract

Experimental and computational investigations are carried out to elucidate the influence of ethanol addition on *n*-heptane auto-ignition in counterflows. An axisymmetric stream of air, temperature gradually increased, is directed onto the surface of an evaporating pool of a liquid fuel. The air-stream temperature at auto-ignition is measured at various strain rates, defined as the axial gradient of the axial component of the flow velocity at the stagnation plane, for *n*-heptane, ethanol, and various *n*-heptane/ethanol mixtures. Critical conditions for auto-ignition are predicted employing the San Diego Mechanism for both fuels and the fuel mixtures, and the results are compared with the measurements. Measurements and predictions show that low-temperature chemistry plays a significant role in promoting auto-ignition of *n*-heptane at low strain rates, but there is insufficient residence time at high strain rates for low-temperature chemistry to take place, so auto-ignition is promoted by high-temperature chemistry. Experimental and computational results show that addition of ethanol inhibits the low-temperature chemistry of *n*-heptane. To identify the responsible elementary steps, computations are performed to identify those that dominate oxygen consumption and that contribute to the temperature rise in the reaction zone for *n*-heptane and *n*-heptane/ethanol mixtures at low strain rates. For *n*-heptane oxygen is consumed primarily by the low-temperature steps that result in ketohydroperoxide; the temperature rise is produced by subsequent low-temperature-chemistry steps. For the mixtures, a key step that consumes O₂ is $\text{O}_2 + \text{CH}_3\text{CHOH} = \text{HO}_2 + \text{CH}_3\text{CHO}$, and the heat release occurs through the classical high-temperature reaction mechanism. Thus, the inhibition of auto-ignition that is observed to occur when ethanol is added to *n*-heptane arises from the competition for oxygen between this step and the low-temperature-chemistry addition of O₂ to the heptyl radical and to the radical arising from the subsequent isomerization, for *n*-heptane.

Keywords: nonpremixed flows; autoignition; heptane; ethanol

1. Introduction

Commercial hydrocarbon fuels are often mixed with alcohols to enable clean and efficient combustion. For this reason, a number of studies have been carried out on mixtures of alcohols with hydrocarbon fuels [1–12]. These studies involved both practical fuel blends and ideal mixtures of components. Foremost among the combustion topics addressed was auto-ignition, since that is a key aspect relative to practical performance. The reader is referred to a useful review for further information concerning the extensive research performed prior to 2019, along with the motivation for the work [1].

Starting from the early investigation of Tipper and Titchard [13], many studies have addressed the influence of alcohols on auto-ignition and combustion of hydrocarbon fuels [4, 5, 10, 11, 13, 14]. Tipper and Titchard [13] investigated the effect of addition of large number of compounds on the cool-flame combustion of *n*-heptane at around 533 K in a static system. Addition of olefins and alcohols was found to inhibit the low-temperature chemistry of *n*-heptane. Goldsborough et al. [3] measured ignition delay times for auto-ignition of mixtures of research-grade gasoline with *iso*-propanol or *iso*-butanol at pressures of 20 and 40 bar and temperatures from 700 to 1000 K. A key finding of this investigation was that at low-temperature/NTC conditions (700–860 K) the iso-alcohols inhibit first-stage reactivity of gasoline. Similar results were obtained for ignition delay times measured in rapid compression machines for mixtures of *n*-butanol and *n*-heptane [5] **and in reflected shock waves [11]**. Addition of *n*-butanol was found to increase the ignition delay times for values of pressure between 15 bar and 30 bar and temperatures between 650 K and 830 K indicating that *n*-butanol inhibits auto-ignition of *n*-heptane [5]. Ignition delay times for auto-ignition of mixtures of alcohols with jet-fuels and petroleum derived fuel were investigated at engine-relevant conditions in a pressure vessel [4] at temperatures between 825 and 900 K and pressures between 6 and 9 MPa. The ignition delay times were found to increase with increasing addition of alcohol, thus confirming that alcohols inhibit low-temperature ignition of hydrocarbon fuels [4]. **Other studies show that addition of ethanol to hydrocarbon fuels reduces emissions of oxides of nitrogen [15, 16] and influences formation of PAH and soot [17]**.

Studies of auto-ignition in rapid-compression machines and shock tubes are primarily concerned with premixed systems and do not consider the influence of flow time on auto-ignition. Recently, Liang et. al [10] carried out an experimental and computational investigation, employing the counterflow configuration, to elucidate the influence of *iso*-butanol on critical conditions of auto-ignition of *n*-decane and *n*-heptane. The temperature of the air stream at auto-ignition, T_{ig} , was measured at

various values of the strain rate. Kinetic modeling was carried out using the comprehensive CRECK chemical–kinetic mechanism. Critical conditions of auto-ignition were predicted and compared with the measurements. Low-temperature chemistry was found to play a significant role in promoting auto-ignition of *n*-decane and *n*-heptane. Experimental data and numerical simulations showed that addition of even small amounts of *iso*-butanol to *n*-decane or *n*-heptane increased the value of T_{ig} at low strain rates, indicating that *iso*-butanol strongly inhibits the low-temperature chemistry of *n*-decane and *n*-heptane. Predicted flame structures showed that the peak values of mole fraction of ketohydroperoxide were significantly reduced when *iso*-butanol was added to *n*-decane, indicating that the kinetic pathway to low temperature ignition is blocked. This observation was confirmed by sensitivity analysis [10].

This previous study [10] did not identify the steps specific to the kinetic model for alcohol combustion that are responsible for inhibiting low-temperature chemistry of *n*-decane and *n*-heptane. Here, an experimental and computational investigation is carried out to characterize the influence of addition of ethanol (C_2H_5OH) on auto-ignition of *n*-heptane (C_7H_{16}), employing the counterflow configuration. Critical conditions for auto-ignition are measured as a function of strain rate for various values of mixture ratios of the fuels. Computations are performed using the San Diego Mechanism [18] and the results are compared with measurements. A key goal of this investigation is to identify those kinetic steps in combustion of ethanol that interfere with low temperature chemistry of *n*-heptane, which has not been achieved in previous investigations.

2. Experiments and Numerical Simulations

2.1. Experimental Apparatus and Procedures

Figure 1 is a schematic illustration of the “condensed-fuel” counterflow configuration employed in this experimental and computational study. In this configuration, an axisymmetric flow of an oxidizer stream made up of oxygen and nitrogen is directed over the surface of an evaporating pool of a liquid fuel in a fuel-cup. It is injected from the oxidizer-duct, the exit of which is the oxidizer boundary. The origin is placed on the axis of symmetry at the surface of the liquid pool, and y is the axial co-ordinate and r the radial co-ordinate and $y = 0$ represents the liquid-gas interface. The distance between the liquid-gas interface and the oxidizer boundary is L . At the oxidizer boundary $y = L$, the magnitude of the injection velocity is V_2 , the temperature T_2 , the density ρ_2 , and the mass fraction of oxygen $Y_{O_2,2}$. Here, subscript 2 represents conditions at the oxidizer boundary. The radial component of the flow velocity at the oxidizer boundary is

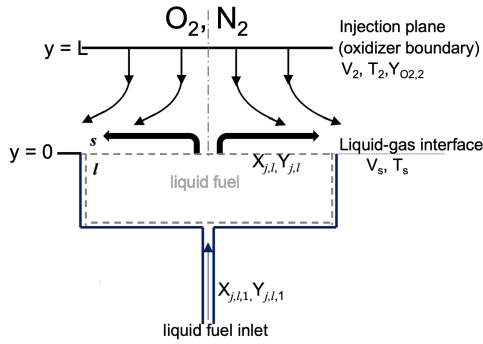


Fig. 1: Schematic illustration of the counterflow configuration. V_2 and V_s are the velocities at the oxidizer boundary and on the gas side of the liquid-gas interface, respectively. T_2 and T_s are the temperatures at the oxidizer boundary and the liquid-gas interface, respectively, and $Y_{O_2,2}$ is the mass fraction of oxygen at the oxidizer boundary.

presumed to be equal to zero. The temperature at the liquid-gas interface is T_s , and the mass averaged velocity on the gas side of the liquid-gas interface is V_s . Here, subscripts s and l , respectively, represent conditions on the gas-side and the liquid-side of the liquid-gas interface. The quantities $X_{j,l}$ and $Y_{j,l}$ are, respectively, the mole-fraction and mass-fraction of the component j in the liquid, and $X_{j,l,1}$ and $Y_{j,l,1}$ are, respectively, the mole-fraction and mass-fraction of the component j in the liquid that is entering the fuel-cup of the counterflow burner. It has been shown previously [19] that the radial component of the flow velocity at the liquid-gas interface is small and can be presumed to be equal to zero. It has been shown that in the asymptotic limit of large Reynolds number the stagnation plane formed between the oxidizer stream and the fuel vapors is close to the liquid-gas interface and a thin boundary layer is established there. The inviscid flow outside the boundary layer is rotational. The local strain rate, a_2 , at the stagnation plane, is given by $a_2 = 2V_2/L$ [19, 20]. Figure 2 is a high-speed photograph of the onset of auto-ignition. When the critical condition of auto-ignition is reached, a thin flame in the form of a disc first appears around the axis of symmetry above the liquid pool and subsequently rapidly covers the entire pool surface.

The counterflow burner is made up of two concentric tubes; an inner ceramic tube, and an outer quartz tube. The ceramic tube has an inner diameter of 26 mm and an outer diameter of 28.6 mm. The oxidizer stream flows through the inner tube and a curtain flow of nitrogen through the outer tube. The distance between the liquid-gas interface and the oxidizer boundary, taking into consideration the thermal expansion of the oxidizer-duct, is $L = 10.5$ mm. A silicon carbide heating element, is placed inside the inner ceramic tube. The surface

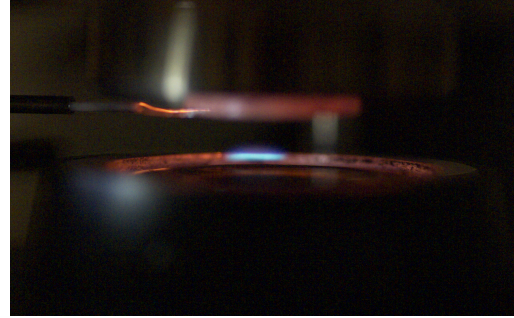


Fig. 2: High-speed photograph of the onset of auto-ignition at strain rate $a_2 = 100 \text{ s}^{-1}$. The fuel is 50% *n*-heptane/50% *n*-heptane. The photo shows the rims of the fuel-cup and the oxidizer-duct, and the thermocouple employed to measure the auto-ignition temperature of the oxidizer stream.

of the heating element can reach a temperature of 1900 K. All gaseous streams are controlled by computer regulated analog mass flow controllers. The velocity of the oxidizer stream at the exit of the duct, V_2 , is presumed to be equal to the ratio of the volumetric flow rate of the oxidizer stream and the cross-section area of the duct. The temperature of the oxidizer at the exit of the duct is measured using a Pt 10% Rh/Pt 13% Rh thermocouple with a wire diameter of 0.21 mm and a bead diameter of 0.457 mm. The thermocouple is held in place by a ceramic holder. The measured temperatures are corrected for radiative heat losses from the thermocouple bead using the Ranz and Marshall correlation for the Nusselt number for convective heat transfer from the gas to the spherical thermocouple bead [21]. The repeatability of temperatures measured by the thermocouple is ± 5 K. Correction for radiative losses from the thermocouple bead are found to be approximately 20 K, therefore the uncertainty in radiation correction is expected to be ± 10 K.

The procedure for measuring critical conditions of auto-ignition is as follows. First, the flow-field is established at a selected value of volumetric flow rate of the oxidizer stream. Liquid fuel is introduced into the fuel-cup. The temperature of the oxidizer stream is gradually increased in small increments, allowing sufficient time for the system to reach steady-state, until auto-ignition takes place. The velocity of the oxidizer stream at the exit of the duct and the corresponding strain rate are calculated from the measured volumetric flow rate. The temperature of air at auto-ignition, T_{ig} is recorded as a function of the strain rate a_2 . The experiment is repeated for different values of the strain rate.

2.2. Numerical Simulations

The computations are performed using Cantera [22] C++ interface with modified boundary condi-

tions for liquid-gas interface of liquid-pool¹. Mix-average transport model is applied to obtained steady-state solutions. At the oxidizer boundary, the injection velocity V_2 , the temperature, T_2 , and the value of $Y_{O_2,2}$ are specified. At the fuel side, equation (1) shows the boundary conditions for species conservation and energy conservation that are applied at the liquid-gas interface.

$$\begin{aligned} \dot{m}Y_{i,s} + j_{i,s} &= 0, \\ \dot{m}Y_{j,s} + j_{j,s} &= \dot{m}Y_{j,l,1}, \\ [\lambda(dT/dy)]_s - \dot{m}\sum_j Y_{j,l}h_{j,l} &= 0, \\ P_{v,j}X_{j,l} - pX_{j,s} &= 0, \end{aligned} \quad (1)$$

and the constraint $\sum_j X_{j,l} - 1 = 0$. Here subscripts i and j , respectively, refer to non-evaporating and evaporating species (specifically components of the liquid fuel), \dot{m} is the mass evaporation rate, $Y_{i,s}$, and $j_{i,s}$ the mass fraction and diffusive flux of the non-evaporating species, $Y_{j,s}$, $X_{j,s}$ and $j_{j,s}$ the mass fraction, mole fraction and diffusive flux of the evaporating species on the gas side of the interface, λ is the thermal conductivity of the gas, and $h_{j,l}$, and $P_{v,j}$, respectively, are the heat of vaporization and vapor pressure of component j on the liquid-side of liquid-gas interface and p the total pressure. The total mass flux of all species, i , on the gas-side of the liquid-gas interface comprises the diffusive flux, $j_{i,s}$, and the convective flux $\dot{m}Y_{i,s}$. The first expression in Eq. (1) imposes the condition that the total mass flux for all species, except for those of the evaporating fuel components, vanishes at the liquid-gas interface. The second expression of Eq. (1) imposes the constraint that the outgoing mass flux of each evaporating component in the liquid from the liquid-gas interface must be equal to the incoming mass flux, specifically the product of \dot{m} and the mass fraction of the species at liquid pool inlet, $Y_{j,l,1}$. The third expression in Eq. (1) is energy balance at the liquid-gas interface, and the fourth expression is Raoult's law relating the mole-fraction of the evaporating species on the gas side to the corresponding mole-fraction in the liquid.

Kinetic modeling is carried out using the San Diego Mechanism [18]. The computer program Cantera is used to compute the flame structure and critical conditions of auto-ignition. The fuels tested are *n*-heptane (HPLC grade, purity $\geq 99\%$), ethanol and mixtures with volumetric composition of 20% *n*-heptane/80% ethanol, 50% *n*-heptane/50% ethanol, and 80% *n*-heptane/20% ethanol. The oxidizer is air. **The saturation vapor, $P_{v,j}$ and the heat of vaporization $h_{j,l}$ in Eq. (1) for any species j are evaluated using the expressions $\log_{10} P_{v,j} = A_{1,j} + B_j/T + C_j \times \log_{10}(T) + D_j \times T + F_j \times T^2$, and $h_{j,l} = A_{2,j}(1 - T/T_{j,cr})^{N_j}$, where the value for the critical temperature $T_{j,cr}$ and the values for the empirical coefficients**

¹<https://github.com/LJ1356/cantera.git>

$A_{1,j}, B_j, C_j, D_j, F_j, A_{2,j}$ and N_j are obtained from [23].

3. Results and Discussion

Figure 3 shows the temperature of the air at

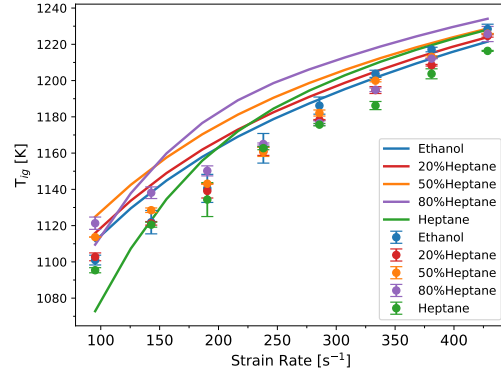


Fig. 3: The temperature of the air at auto-ignition, T_{ig} , of *n*-heptane, ethanol and mixtures of *n*-heptane and ethanol by volume as a function of strain-rate, a_2 . The symbols represent experimental data and the lines are predictions. The uncertainty in experimental data is ± 10 K.

auto-ignition, T_{ig} , as a function of strain-rate, a_2 , for *n*-heptane, ethanol and mixtures of these fuels. In this figure, the symbols represent experimental data and the lines are predictions. At low strain rates, around $a_2 = 95 \text{ s}^{-1}$, measurements show that *n*-heptane is easiest to ignite because it has the lowest value of T_{ig} and the value of T_{ig} increases in the order, ethanol, 20% *n*-heptane/80% ethanol, 50% *n*-heptane/50% ethanol, and 80% *n*-heptane/20% ethanol. It is noteworthy that at low strain rates, all mixtures have higher values of T_{ig} than the components of the mixture. At low strain rates computations show a similar trend where *n*-heptane is easiest to ignite followed by ethanol and 80% *n*-heptane/20% ethanol that have nearly the same value of T_{ig} , while the mixtures 20% *n*-heptane/80% ethanol, and 50% *n*-heptane/50% ethanol have values of T_{ig} that are higher than those for *n*-heptane and ethanol. Moreover, experimental data and predictions show that at low strain rates addition of a small amount (20%) of ethanol increases T_{ig} by a significant amount from that for *n*-heptane, indicating that addition of ethanol strongly inhibits the low-temperature chemistry of *n*-heptane. This behavior is similar to that observed in a previous investigation where *iso*-butanol was found to inhibit low-temperature chemistry of *n*-heptane and *n*-decane [10]. Figure 3 shows that at high strain rates the measured value of T_{ig} for *n*-heptane is the lowest and T_{ig} for the mixtures are nearly the same as that for ethanol and the differences are well within experimental uncertainties. At high strain rates the predictions show that T_{ig} for ethanol is

the lowest followed by 20% *n*-heptane/80% ethanol, 50% *n*-heptane/50% ethanol, *n*-heptane and 80% *n*-heptane/20% ethanol. Thus, the order of increase in values of T_{ig} in the experiment and predictions do not match at high strain rates. **In general, the quantitative agreement between the measurements and predictions are within experimental uncertainty. The deviations can also arise from uncertainties in the kinetic model for ethanol and requires further investigation.**

Following previous investigation where *iso*-butanol was found to inhibit low-temperature chemistry of *n*-heptane and *n*-decane [10], computations were carried out with the complete mechanism and with the low-temperature reactions of *n*-heptane removed from the kinetic model and the results are shown in Fig. 4. For *n*-heptane, at low strain

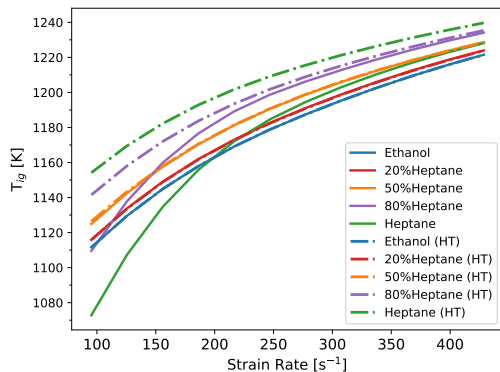


Fig. 4: The predicted temperature of the air at auto-ignition, T_{ig} , of *n*-heptane, ethanol and mixtures of *n*-heptane/ethanol with percent volume ratios of 80/20, 50/50, and 20/80, as a function of strain-rate, a_2 . The figure shows predictions with the complete kinetic mechanism and those with low-temperature chemistry removed (HT).

rates, the value of T_{ig} calculated neglecting low-temperature chemistry is significantly larger than that predicted using complete kinetic model. For the mixture with 80% *n*-heptane/20% ethanol T_{ig} calculated neglecting low-temperature chemistry is higher than that calculated using the complete model, but the differences are not as large as those for *n*-heptane. Thus, some influence of low-temperature chemistry on auto-ignition is still present in this mixture. It is noteworthy that for the mixtures 20% *n*-heptane/80% ethanol and 50% *n*-heptane/50% ethanol the values of T_{ig} calculated with and without low-temperature chemistry are nearly the same, indicating that ethanol has inhibited the low-temperature chemistry of *n*-heptane for these mixtures.

Figures 5, 6, and 7 respectively, show predicted profiles of heat release, main elementary steps that consume oxygen, and the main elementary steps

that contribute to the rise in temperature, close to auto-ignition of *n*-heptane at low strain rate, $a_2 = 95 \text{ s}^{-1}$. The liquid gas interface is at the

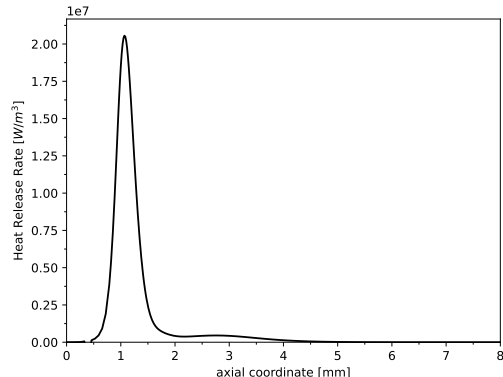


Fig. 5: Predicted profile of heat release for *n*-heptane. Oxidizer temperature, $T_2 = 1000 \text{ K}$, strain rate $a_2 = 95 \text{ s}^{-1}$.

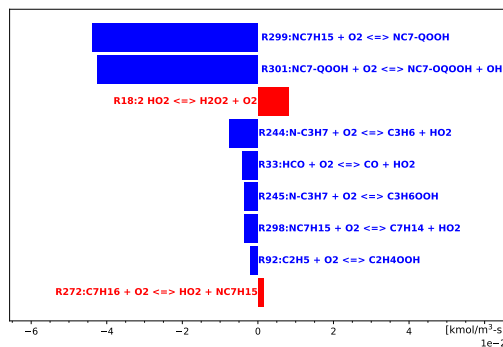


Fig. 6: Key elementary steps that consume oxygen for *n*-heptane at the location of maximum heat release indicated in Fig. 5 ($y = 1.07 \text{ mm}$). Oxidizer temperature, $T_2 = 1000 \text{ K}$, strain rate $a_2 = 95 \text{ s}^{-1}$. Blue represents consumption and red formation.

axial location, $y = 0$ and the exit of the duct at $y = 10.5 \text{ mm}$. Figure 5 shows that the profile of heat release has two peaks, one around $y \approx 1 \text{ mm}$ and the other around $y \approx 3 \text{ mm}$. The first peak, where low-temperature chemistry is expected to take place, is significantly higher than the second peak, where high temperature chemistry is expected to take place. Figures 6 shows that O_2 is consumed primarily by the low-temperature reactions of *n*-heptane and Fig. 7 shows that temperature rise is primarily due to low-temperature kinetic steps. Thus, for *n*-heptane at low strain rates auto-ignition is promoted by low-temperature chemistry.

Figure 8 shows predicted profile of heat release close to auto-ignition of ethanol at low strain rate, $a_2 = 95 \text{ s}^{-1}$ and $T_2 = 1100 \text{ K}$. In contrast to the profile of heat-release for *n*-heptane shown in Fig. 5 the profile of heat release for ethanol

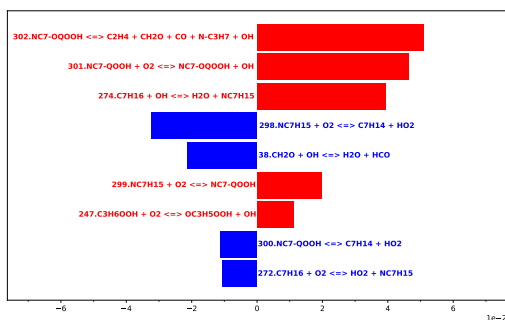


Fig. 7: Key elementary steps that contribute to the rise of temperature for *n*-heptane at the location of maximum heat release indicated in Fig. 5 ($y = 1.07$ mm). Oxidizer temperature, $T_2 = 1000$ K, strain rate $a_2 = 95$ s $^{-1}$. Blue represents reactions that decrease temperature and red reactions that increase temperature

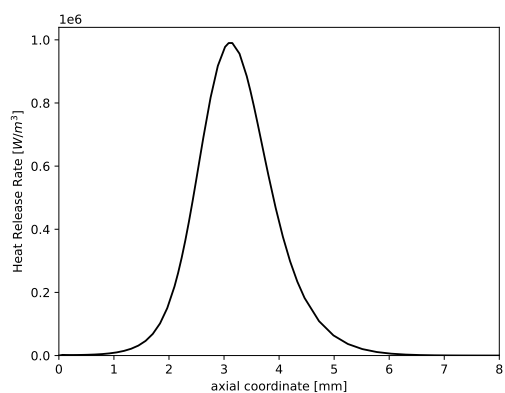


Fig. 8: Predicted profile of heat release for ethanol. Oxidizer temperature, $T_2 = 1100$ K, strain rate $a_2 = 95$ s $^{-1}$.

shows only one peak around 3 mm. This is consistent with the accepted point of view that unlike *n*-heptane, ethanol does not have separate low-temperature and high-temperature chemistry.

Figures 9, 10, and 11, respectively, show the profile of heat release, main elementary steps that consume oxygen, and the main elementary steps that contribute to the rise in temperature for mixtures with volumetric composition of 50% *n*-heptane/50% ethanol. The oxidizer temperature, $T_2 = 1100$ K and strain rate $a_2 = 95$ s $^{-1}$. The heat release profile in Fig. 9 shows two peaks at approximately the same locations as those in Fig. 5, however, in Fig. 9 the peak further away from the liquid-gas interface, where high-temperature reactions are expected to take place, is higher than the one closer to the liquid-gas interface. Figure 10 shows that a key step that consumes O_2 is $O_2 + CH_3CHOH = HO_2 + CH_3CHO$. Figure 11 shows that the temperature rise is primarily due to the reaction $H + O_2 = OH + O$ and $OH + OH = H_2O_2 + M$ which is different from that shown in Fig. 7 where

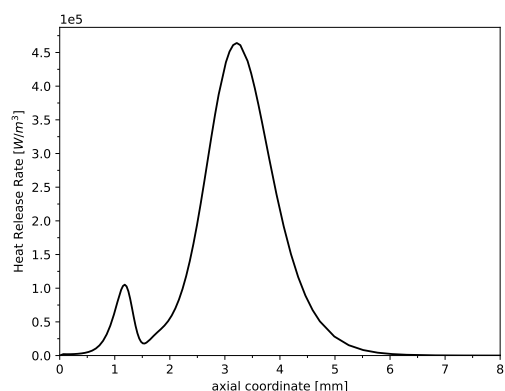


Fig. 9: Predicted profile of heat release for mixtures with volumetric composition of 50% *n*-heptane/50% ethanol. Oxidizer temperature, $T_2 = 1100$ K, strain rate $a_2 = 95$ s $^{-1}$.

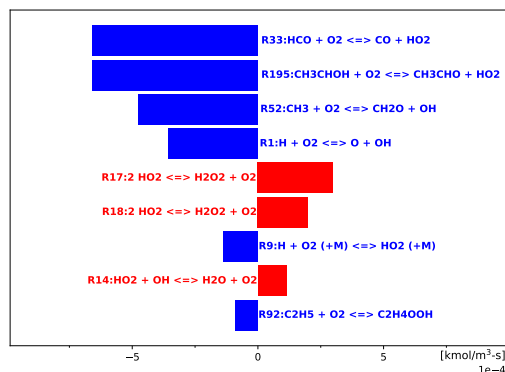


Fig. 10: Key elementary steps that consume oxygen for mixtures with volumetric composition of 50% *n*-heptane/50% ethanol at the location of maximum heat release indicated in Fig. 9 ($y = 3.22$ mm). Oxidizer temperature, $T_2 = 1100$ K, strain rate $a_2 = 95$ s $^{-1}$. Blue represents consumption and red formation

the temperature rise is from the low-temperature chemistry of *n*-heptane. Thus, auto-ignition for this mixture is primarily advanced by high-temperature reactions.

To test if competition between kinetic steps that consume O_2 in the mechanism of *n*-heptane and ethanol are responsible for inhibition of auto-ignition at low strain rates, computations were performed with the step $O_2 + CH_3CHOH = HO_2 + CH_3CHO$ removed from the kinetic model and the results are shown in Fig. 12. In this figure, the solid lines represent predictions with the complete kinetic mechanism and the broken line predictions with the step $O_2 + CH_3CHOH = HO_2 + CH_3CHO$ removed. As expected, Fig. 12 shows that removal of this step does not change the critical conditions of auto-ignition of *n*-heptane but decreases the value of the auto-ignition temperature, T_{ig} , of ethanol by a significant amount between 50 and 75 K. It is noteworthy when this

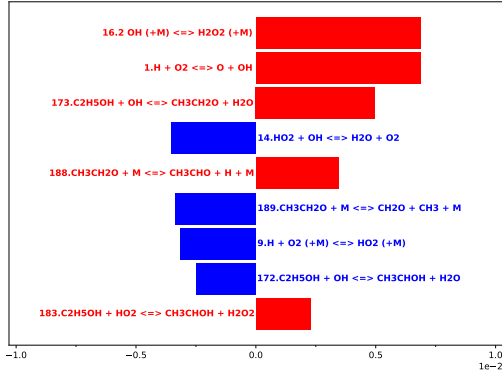


Fig. 11: Key elementary steps that contribute to the rise of temperature for mixtures with volumetric composition of 50% *n*-heptane/50% ethanol at the location of maximum heat release indicated in Fig. 9 ($y = 3.22$ mm). Blue represents reactions that decrease temperature and red reactions that increase temperature.

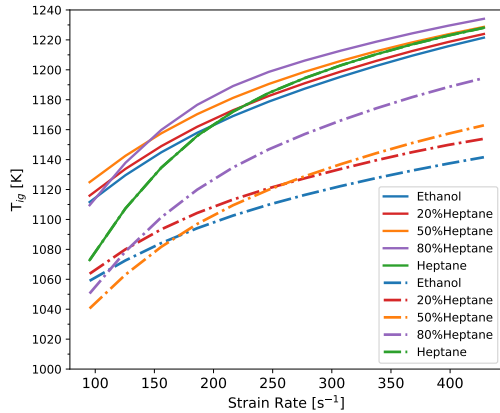


Fig. 12: The predicted temperature of the air at auto-ignition, T_{ig} , of *n*-heptane, ethanol and mixtures of *n*-heptane/ethanol with percent volume ratios of 80/20, 50/50, and 20/80, as a function of strain-rate, a_2 . The solid lines represent predictions with the complete kinetic mechanism, and the broken lines predictions with the step $O_2 + CH_3CHOH = HO_2 + CH_3CHO$ removed.

step is removed, at low strain rates, the value of T_{ig} for the mixture 50% *n*-heptane/50% ethanol is lower than that for 20% *n*-heptane/80% ethanol, while this order is reversed at high strain rates. This behavior is a consequence of the fact that at low strain rates low-temperature chemistry is active, hence the mixture with the larger amount of *n*-heptane has a lower value of T_{ig} while at high strain rates where low-temperature chemistry does not take place the order is reversed because the value of T_{ig} for *n*-heptane is larger than that for ethanol [19, 24]. Predictions including this step show that the value of T_{ig} for 50% *n*-heptane/50% ethanol is larger than that for 20% *n*-heptane/80% ethanol for all values of the strain rate. Thus, low-temperature chemistry

of *n*-heptane that was suppressed when ethanol was added is restored when $O_2 + CH_3CHOH = HO_2 + CH_3CHO$ is removed. At high strain rates, Fig. 12 shows that in the predictions with and without the step $O_2 + CH_3CHOH = HO_2 + CH_3CHO$, the value of T_{ig} increases with increasing amounts of *n*-heptane in the mixture because there is insufficient residence time for low-temperature chemistry to be active, therefore exclusion of this step does not have an influence on the critical conditions of auto-ignition.

Figures 13, 14, and 15, respectively, show profiles of heat release, main elementary steps that consume oxygen, and the main elementary steps that contribute to the rise in temperature predicted at conditions close to auto-ignition for mixtures with volumetric composition of 50% *n*-heptane/50% ethanol with step $O_2 + CH_3CHOH = HO_2 + CH_3CHO$ removed with $T_2 = 1000$ K, strain rate $a_2 = 95 s^{-1}$.

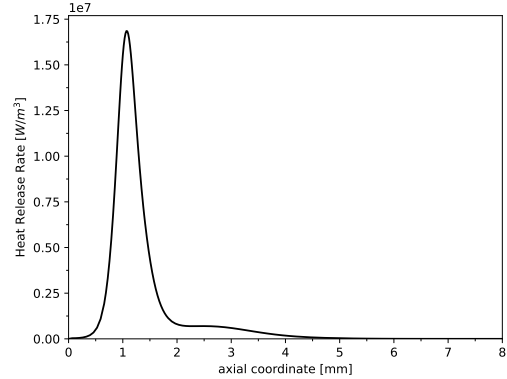


Fig. 13: Predicted profile of heat release for mixtures with volumetric composition of 50% *n*-heptane/50% ethanol with step $O_2 + CH_3CHOH = HO_2 + CH_3CHO$ removed and oxidizer temperature, $T_2 = 1000$ K, strain rate $a_2 = 95 s^{-1}$.

Comparing the profile in of Fig. 13 with that in Fig. 9 shows that both figures show two peaks. In the former, the peak closer to the liquid-gas boundary, where low-temperature chemistry is active, is more prominent while in the latter the peak further away from the liquid-gas boundary is more prominent. This indicates that low-temperature chemistry of *n*-heptane is restored when $O_2 + CH_3CHOH = HO_2 + CH_3CHO$ is removed. Figure 10 shows that O_2 is primarily consumed in the step $O_2 + CH_3CHOH = HO_2 + CH_3CHO$, while Fig. 14 shows that O_2 is consumed by the low-temperature steps of *n*-heptane. Moreover, Fig. 11 shows that the temperature rise in the reaction zone is primarily from high temperature chemistry, while Fig. 15 shows that the temperature increase is from the low-temperature reactions of *n*-heptane. These observations provide further confirmation that the step, $O_2 + CH_3CHOH = HO_2 + CH_3CHO$, competes with O_2 consumption by low-temperature reactions of *n*-heptane. As

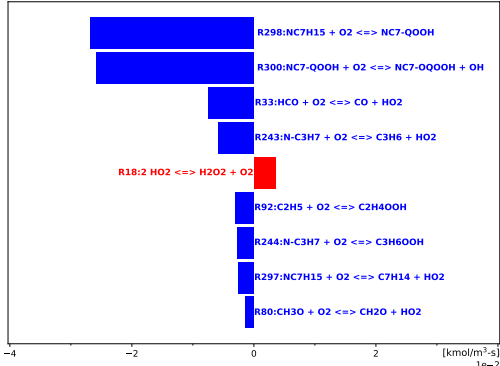


Fig. 14: Key elementary steps that consume oxygen for mixtures with volumetric composition of 50% *n*-heptane/50% ethanol at the location of maximum heat release indicated in Fig. 13 ($y = 1.1$ mm) with step $O_2 + CH_3CHOH = HO_2 + CH_3CHO$ removed and oxidizer temperature, $T_2 = 1000$ K, strain rate $a_2 = 95$ s $^{-1}$. Blue represents consumption and red formation

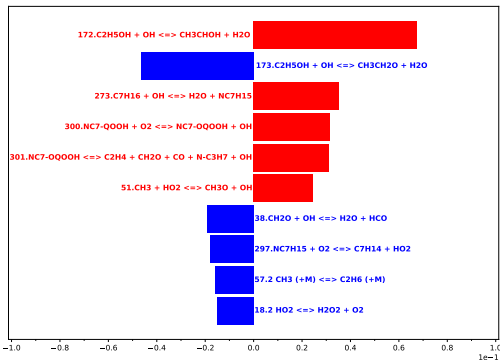


Fig. 15: Key elementary steps that contribute to the rise of temperature for mixtures with volumetric composition of 50% *n*-heptane/50% ethanol at the location of maximum heat release indicated in Fig. 13 ($y = 1.1$ mm) with step $O_2 + CH_3CHOH = HO_2 + CH_3CHO$ removed and oxidizer temperature, $T_2 = 1000$ K, strain rate $a_2 = 95$ s $^{-1}$. Blue represents reactions that decrease temperature and red reactions that increase temperature.

a consequence, the low-temperature reactions of *n*-heptane are suppressed when ethanol is added.

Cheng et al. [14] studied auto-ignition behavior of gasoline/ethanol blends in a rapid compression machine. In the low-temperature regime ethanol was found to retard first stage and main ignition delay times and suppress the rates and extents of low-temperature heat release. Qualitatively this is similar to observations reported here where addition of ethanol not only increases the auto-ignition temperature at low strain rates but also decreases the level of heat release in the region where low-temperature chemistry is expected to take place.

4. Concluding Remarks

This work has identified the key mechanism through which ethanol addition inhibits the low-temperature auto-ignition process of *n*-heptane. Just as the heptyl radical exhibits an attractive site for addition of an oxygen molecule, so does the radical produced by H-atom abstraction from the ethanol site adjacent to the hydroxyl exhibit sufficient attraction for oxygen molecules to compete favorably with heptyl, yielding hydroperoxyl plus a stable molecule. By depriving heptyl and its isomerized oxygen-addition product (often denoted by QOOH in the literature) from a sufficient supply of oxygen molecules, the ethanol-generated radical turns off the low-temperature path in *n*-heptane, thereby increasing its auto-ignition time.

This same mechanism is likely to prevail for higher alcohols, as well, thereby contribution to other perhaps unexpected experimental results. Future research involving these higher alcohols, as well as different normal alkanes, would be worthwhile, to determine how generally relevant this type of new mechanism may be. Implications may be expected on auto-ignition behaviors of developing environment-friendly new fuels designed to mitigate detrimental climate effect.

References

- [1] S. M. Sarathy, A. Farooq, G. T. Kalghatgi, Recent progress in gasoline surrogate fuels, *Progress in Energy and Combustion Science* 65 (2018) 67–108.
- [2] I. Gorbatenko, A. S. Tomlin, M. Lawes, R. F. Cracknell, Experimental and modelling study of the impacts of *n*-butanol blending on the auto-ignition behaviour of gasoline and its surrogate at low temperatures, *Proceedings of the Combustion Institute* 37 (2019) 501–509.
- [3] S. S. Goldsborough, S. Cheng, D. Kang, C. Saggese, S. W. Wagnon, W. J. Pitz, Effects of isoalcohol blending with gasoline on autoignition behavior in a rapid compression machine: Isopropanol and isobutanol, *Proceedings of the Combustion Institute* 38 (2021) 5655–5664.
- [4] E. K. Mayhew, C. M. Mitsingas, V. D. Coburn, J. E. Temme, C. M. Kweon, Effects of fuel blending on first stage and overall ignition processes, *Proceedings of the Combustion Institute* 38 (2021) 5733–5740.
- [5] Z. Yang, Y. Qian, X. Yang, Y. Wang, Y. Wang, Z. Huang, X. Lu, Autoignition of *n*-butanol/*n*-heptane blend fuels in a rapid compression machine under low-to-medium temperature ranges, *Energy Fuels* 27 (2013) 7800–7808.
- [6] O. Welz, J. D. Savee, A. J. Eskola, L. Sheps, D. L. Osborn, C. A. Taatjes, Low-temperature combustion chemistry of biofuels: Pathways in the low-temperature (550–700 K) oxidation chemistry of isobutanol and tert-butanol, *Proceedings of the Combustion Institute* 34 (2013) 5655–5664.
- [7] Y. Xu, C. T. Avedisian, Combustion of *n*-butanol, gasoline, and *n*-butanol/gasoline mixture droplets, *Energy & Fuels* 29 (2015) 3467–3475.

- [8] A. Dalili, J. D. Brunson, S. Guo, M. Turello, F. Pizzetti, L. Badiali, C. T. Avedisian, K. Seshadri, A. Cuoci, F. A. Williams, A. Frassoldati, M. C. Hicks, The role of composition in the combustion of *n*-heptane/iso-butanol mixtures: Experiments and detailed modelling, *Combustion Theory and Modelling* 24 (2020) 1002–1020.
- [9] A. Cuoci, C. T. Avedisian, J. D. Brunson, S. Guo, A. Dalili, Y. Wang, M. Mehl, A. Frassoldati, K. Seshadri, J. E. Dec, D. Lopez-Pintor, Simulating combustion of a seven-component surrogate for a gasoline/ethanol blend including soot formation and comparison with experiments, *Fuel* 288 (2021) 119451.
- [10] L. Ji, A. Cuoci, A. Frassoldati, M. Mehl, T. Avedisian, K. Seshadri, Experimental and computational investigation of the influence of iso-butanol on autoignition of *n*-decane and *n*-heptane in non-premixed flows, *Proceedings of the Combustion Institute* 39 (2023) 2007–2015.
- [11] J. Zhang, S. Niu, Y. Zhang, C. Tang, X. Jiang, E. Hu, Z. Huang, Experimental and modeling study of the auto-ignition of *n*-heptane/*n*-butanol mixtures, *Combustion and Flame* 160 (1) (2013) 31–39. doi:<https://doi.org/10.1016/j.combustflame.2012.09.006>.
- [12] Y. Liu, J. Ding, Combustion chemistry of *n*-heptane/ethanol blends: a reaxff study, *Molecular Simulation* 47 (1) (2021) 37–45. doi:[10.1080/08927022.2020.1862416](https://doi.org/10.1080/08927022.2020.1862416).
- [13] C. F. H. Tipper, A. Titehard, The effect of additives on the cool flame combustion of *n*-heptane, *Combustion and Flame* 16 (1971) 223–232.
- [14] S. Cheng, D. Kang, A. Fridlyand, S. S. Goldborough, C. Saggese, S. Wagnon, M. J. McNenly, M. Mehl, W. J. Pitz, D. Vuilleumier, Autoignition behavior of gasoline/ethanol blends at engine-relevant conditions, *Combustion and Flame* 216 (2020) 369–384. doi:<https://doi.org/10.1016/j.combustflame.2020.02.032>.
- [15] A. Bögrek, C. Haşimoğlu, A. Calam, B. Aydoğan, Effects of *n*-heptane/toluene/ethanol ternary fuel blends on combustion, operating range and emissions in premixed low temperature combustion, *Fuel* 295 (2021) 120628. doi:<https://doi.org/10.1016/j.fuel.2021.120628>.
- [16] M. Lubrano Lavadera, C. Brackmann, G. Capriolo, T. Methling, A. A. Konnov, Measurements of the laminar burning velocities and no concentrations in neat and blended ethanol and *n*-heptane flames, *Fuel* 288 (2021) 119585. doi:<https://doi.org/10.1016/j.fuel.2020.119585>.
- [17] F. Yan, L. Xu, Y. Wang, S. Park, S. M. Sarathy, S. H. Chung, On the opposing effects of methanol and ethanol addition on pah and soot formation in ethylene counterflow diffusion flames, *Combustion and Flame* 202 (2019) 228–242. doi:<https://doi.org/10.1016/j.combustflame.2019.01.020>.
- [18] The San Diego Mechanism, <http://combustion.ucsd.edu> (2009).
- [19] K. Seshadri, S. Humer, R. Seiser, Activation-energy asymptotic theory of autoignition of condensed hydrocarbon fuels in non-premixed flows with comparison to experiment, *Combustion Theory and Modelling* 12 (2008) 831–855.
- [20] K. Seshadri, F. A. Williams, Laminar flow between parallel plates with injection of a reactant at high Reynolds number, *International Journal of Heat and Mass Transfer* 21 (2) (1978) 251–253.
- [21] T. L. Bergman, A. S. Lavine, F. P. Incropera, D. P. Dewitt, *Fundamentals of Heat and Mass Transfer*, 8th Edition, Wiley, New York, 2017.
- [22] Cantera: An object-oriented software toolkit for chemical kinetics, thermodynamics, and transport processes., version 3.0.0 (2023). doi:[10.5281/zenodo.8137090](https://doi.org/10.5281/zenodo.8137090). URL <https://www.cantera.org/>
- [23] C. L. Yaws, *Yaws' Handbook of Thermodynamic and Physical Properties of Chemical Compounds*, Knovel, 2003.
- [24] R. Grana, K. Seshadri, A. Cuoci, U. Niemann, T. Faravelli, E. Ranzi, Kinetic modelling of extinction and autoignition of condensed hydrocarbon fuels in non-premixed flows with comparison to experiment, *Combustion and Flame* 159 (2012) 130–141.